

A Classification of Positive-Curvature Discrete Einstein Metrics on Trees

Haoxuan Cheng*

Abstract

For a weighted tree, the Lin–Lu–Yau Ricci curvature admits an explicit formula in terms of the edge weights. Consequently, the constant-curvature equation is equivalent to an eigenvalue problem for an edge-indexed Ricci matrix R_T . Building on the spectral characterization of discrete Einstein metrics on trees, we classify all finite trees whose discrete Einstein metric has positive curvature, equivalently all trees satisfying $\lambda_{\max}(R_T) < 0$. For caterpillars with spine order $m \geq 12$, this occurs precisely for the endpoint families $T_m(a, 0, \dots, 0, b)$ with $1 \leq a, b \leq 3$ and $(a, b) \neq (3, 3)$. The remaining cases $3 \leq m \leq 11$ are settled by an exact finite verification using rational characteristic polynomials and Sturm root counts. We also determine the zero level set $\lambda_{\max}(R_T) = 0$: among caterpillars, it consists of the stable family $(3, 0, \dots, 0, 3)$ together with nine exceptional short-spine caterpillars, while S_3^2 is the unique non-caterpillar zero example.

1 Introduction

The problem of finding Einstein metrics is one of the central problems in Riemannian geometry [1]. A Riemannian metric g is Einstein if

$$\text{Ric}(g) = \kappa g$$

for a constant κ . In the smooth setting, the Einstein equation is closely related to the fixed points of the normalized Ricci flow [2, 3].

Several discrete analogues of Ricci curvature have been introduced on graphs, including Ollivier Ricci curvature and the Lin–Lu–Yau curvature [4, 5]; see also [6, 7]. These curvatures are connected with analytic and geometric properties such as spectrum, diameter, and rigidity; see for instance [8, 10, 12]. They have also led to applications in graph coloring, community detection, and network geometry, as well as to structural results for idleness functions, graph products, and special graph families; see [9, 11, 12, 13, 14, 15, 16, 17, 18, 19, 20].

Let $G = (V, E, w)$ be a finite weighted graph with positive edge weight $w : E \rightarrow \mathbb{R}_{>0}$. For an edge $xy \in E$, denote by κ_{xy} its Lin–Lu–Yau Ricci curvature. We call (G, w) a discrete Einstein graph if κ_{xy} is independent of xy . For trees, the curvature admits a closed formula. After multiplying by the edge weights, the discrete Einstein condition therefore becomes a finite-dimensional linear eigenvalue problem.

In addition to static curvature, one can also study geometric evolution on graphs. For weighted graphs, Ollivier Ricci flow has been introduced and analyzed in [21, 22], while for trees a detailed long-time analysis was recently obtained in [23]. In the recent work of Bai and Hua [24], the associated edge-indexed matrix R_T was introduced. We call R_T the Ricci matrix of the tree.

*School of Mathematical Sciences, Fudan University. Email: hxcheng25@m.fudan.edu.cn.

Perron–Frobenius theory yields a unique positive eigenvector of R_T , up to scaling. This eigenvector is precisely the discrete Einstein metric on the tree. Thus every finite tree admits a unique discrete Einstein metric, while the sign of its curvature is governed by the largest eigenvalue of R_T . Equivalently, the positive-curvature problem becomes the problem of classifying finite trees satisfying

$$\lambda_{\max}(R_T) < 0.$$

The starting point of the present paper is the implication proved in [24]:

$$\lambda_{\max}(R_T) < 0 \implies T \text{ is a caterpillar.}$$

That paper also established the spectral characterization of discrete Einstein metrics on trees, several attachment monotonicity results, and the stable zero family obtained from the symmetric double star; see [24, Theorem 1.2, Propositions 3 and 7, Proposition 8]. The converse of the implication is false. The natural next question, posed in [24], is therefore to determine exactly which caterpillars satisfy $\lambda_{\max}(R_T) < 0$, or equivalently, which trees carry a positive-curvature discrete Einstein metric.

For a caterpillar, we write $T_m(a)$ for the tree with spine order m and leaf-count sequence

$$a = (a_1, \dots, a_m), \quad a_1, a_m \geq 1, \quad a_i \geq 0,$$

where a_i denotes the number of leaves attached to the i th spine vertex.

Our main result is the following theorem.

Theorem 1.1. *Let T be a finite tree.*

- (i) *The discrete Einstein metric on T has positive curvature if and only if $\lambda_{\max}(R_T) < 0$. If $\lambda_{\max}(R_T) < 0$, then T is a caterpillar.*
- (ii) *Let $T = T_m(a)$ be a caterpillar. Then $\lambda_{\max}(R_T) < 0$ if and only if one of the following holds:*
 - (a) $m = 1$;
 - (b) $m = 2$ and $(a_1 - 1)(a_2 - 1) < 4$;
 - (c) $3 \leq m \leq 11$ and a lies in the downward closure of the maximal elements listed in Table 1;
 - (d) $m \geq 12$ and

$$a = (a_1, 0, \dots, 0, a_m), \quad 1 \leq a_1, a_m \leq 3, \quad (a_1, a_m) \neq (3, 3).$$

- (iii) *One has $\lambda_{\max}(R_T) = 0$ if and only if one of the following holds:*

- (a) $T = S_3^2$;
- (b) $T = T_m(a)$ is a caterpillar with

$$a = (3, 0, \dots, 0, 3);$$

- (c) $T = T_m(a)$ is a caterpillar and, up to reversal, a is one of the parameters listed in Table 2.

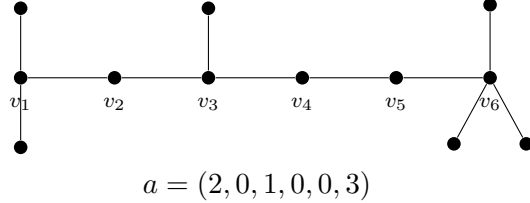


Figure 1: The caterpillar $T_6(2, 0, 1, 0, 0, 3)$ encoded by the leaf-count sequence $a = (2, 0, 1, 0, 0, 3)$.

Thus Theorem 1.1 completes the classification problem posed in [24].

In Section 2, we restate the negative and zero classifications separately as Theorems 2.1 and 2.2, after introducing the Ricci matrix and the caterpillar quotient equations.

The contribution of the present work splits naturally into four parts. The cases $m = 1$ and $m = 2$, namely stars and double stars, are treated separately. For caterpillars with long spine, namely $m \geq 12$, we combine a Rayleigh-quotient argument for leaf attachment with an explicit Schur-complement analysis to reduce the problem to the endpoint families. The remaining finite range $3 \leq m \leq 11$ is then resolved by an exact finite verification, recorded in the tables below. The same leaf-attachment argument also identifies the unique non-caterpillar tree in the zero level set, namely S_3^2 . Since the Einstein curvature is $\kappa = -\lambda_{\max}(R_T)$, this is exactly a classification of positive-curvature discrete Einstein metrics on trees.

The paper is organized as follows. Section 2 introduces the Ricci matrix, the caterpillar quotient equations, and the main classification statements. Section 3 gives the leaf-attachment argument, the initial cases $m = 1, 2$, and the non-caterpillar reduction. Section 4 treats the long-spine caterpillar case. Section 5 handles the remaining short-spine range by exact finite verification. Section 6 discusses the infinite-tree setting. The appendices contain the finite boundary tables, representative zero vectors, and the boundary-generation check.

2 Preliminaries

Throughout the paper, all trees are finite, simple, connected, and undirected. For a tree $T = (V, E)$ and a vertex $v \in V$, let d_v be the degree of v . A vertex of degree one is called a leaf or pendant vertex. An edge incident to a leaf is called a leaf edge. An edge whose two endpoints both have degree at least two is called an internal edge.

Definition 2.1 (Star and caterpillar). For $k \geq 2$, a star S_k is a tree with exactly one internal vertex and k edges; we also include the degenerate case $S_1 = K_2$. A caterpillar is a tree for which removing all leaves leaves a path. This remaining path is called the spine. In our parametrization, the spine vertices are denoted v_1, \dots, v_m , and a_i is the number of leaves attached to v_i .

We write S_3^2 for the tree obtained by subdividing each edge of the three-leaf star S_3 once. Equivalently, S_3^2 has a central vertex of degree three, and each of its three incident edges is extended by one additional edge to a leaf.

We recall that for a caterpillar in canonical form one writes

$$a = (a_1, \dots, a_m), \quad a_1, a_m \geq 1, \quad a_i \geq 0.$$

The corresponding tree is denoted by $T_m(a)$. Reversing a gives an isomorphic tree, so tables below list only one representative up to reversal. The case $m = 1$ is the star S_{a_1} and is treated separately below.

2.1 The Ricci curvature formula on trees

Let $T = (V, E, w)$ be a weighted tree with $w_e > 0$ for every edge e . For a vertex v , set

$$S_v = \sum_{u \sim v} w_{uv}.$$

For an edge $e = xy$, the Lin–Lu–Yau curvature on a tree is

$$\kappa_{xy} = - \left(\frac{S_x - 2w_{xy}}{d_x w_{xy}} + \frac{S_y - 2w_{xy}}{d_y w_{xy}} \right).$$

Therefore the condition $\kappa_{xy} \equiv \kappa$ is equivalent, after multiplying the equation by w_{xy} , to

$$-\kappa w_{xy} = \frac{S_x - 2w_{xy}}{d_x} + \frac{S_y - 2w_{xy}}{d_y}.$$

This is precisely an eigenvalue equation for the Ricci matrix below, introduced in [24, Definition 1].

Definition 2.2 (Ricci matrix). For a finite tree $T = (V, E)$, define the edge-indexed matrix $R_T \in \mathbb{R}^{E \times E}$ by

$$(R_T)_{e,e} = - \left(\frac{1}{d_x} + \frac{1}{d_y} \right), \quad e = \{x, y\},$$

and, for distinct edges $e \neq f$,

$$(R_T)_{e,f} = \begin{cases} 1/d_z, & e \cap f = \{z\}, \\ 0, & e \cap f = \emptyset. \end{cases}$$

For an edge weight vector $w = (w_e)_{e \in E}$, the above curvature formula gives

$$R_T w = \lambda w, \quad \lambda = -\kappa.$$

The matrix R_T is real symmetric and Metzler. Since the line graph $L(T)$ is connected, $R_T + cI$ is irreducible and nonnegative for all sufficiently large c . Perron–Frobenius theory implies that $\lambda_{\max}(R_T)$ is simple and has a strictly positive eigenvector. Consequently every finite tree has a unique discrete Einstein metric up to scaling, and its curvature is

$$\kappa = -\lambda_{\max}(R_T).$$

This recovers the spectral characterization proved in [24, Theorem 1.2].

Remark 2.1 (Schrödinger viewpoint). Equivalently, R_T may be viewed as a weighted Schrödinger operator on the line graph $L(T)$. This viewpoint is useful near the zero level set $\lambda_{\max} = 0$, where degree-two chains satisfy a zero-energy second-order recurrence.

2.2 The caterpillar quotient equations

We record the finite system used throughout the classification. In this subsection assume $m \geq 2$, since the case $m = 1$ is a star and is treated separately. Let $T_m(a)$ be a caterpillar with spine vertices v_1, \dots, v_m . Write $s_j = v_j v_{j+1}$ for the spine edge between v_j and v_{j+1} , and put

$$q_i = \begin{cases} 1, & i = 1, m, \\ 2, & 2 \leq i \leq m-1, \end{cases} \quad d_i = q_i + a_i.$$

On the Perron eigenspace, all pendant edges attached to the same spine vertex have the same value. We denote the value on s_j by x_j , and the common value of the pendant edges at v_i by y_i when $a_i > 0$. Set

$$X_i = \mathbf{1}_{i>1}x_{i-1} + \mathbf{1}_{i<m}x_i + a_i y_i.$$

The eigenvalue equation $R_T w = \lambda w$ is equivalent to

$$\lambda x_j = \frac{X_j - 2x_j}{d_j} + \frac{X_{j+1} - 2x_j}{d_{j+1}}, \quad 1 \leq j \leq m-1,$$

and, for every i with $a_i > 0$,

$$\lambda y_i = -y_i + \frac{X_i - 2y_i}{d_i}.$$

Let \mathcal{U} denote the subspace of edge functions that are constant on each orbit of sibling pendant edges. The preceding equations are the matrix form of $R_T|_{\mathcal{U}}$ in the natural, generally non-orthonormal common-value coordinates. Since R_T commutes with permutations of sibling pendant edges and the Perron eigenvalue is simple, the Perron eigenvector lies in \mathcal{U} . Hence $\lambda_{\max}(R_T)$ is the largest eigenvalue of this restricted coordinate matrix.

This coordinate matrix has the correct spectrum on \mathcal{U} , but is not symmetric in general. For Schur complements, inertia, and Sylvester's criterion, one must pass to an orthonormal orbit basis. For every i with $a_i > 0$, let

$$u_i = \frac{1}{\sqrt{a_i}} \sum_{e \text{ pendant at } v_i} e$$

be the normalized pendant-orbit vector, and write

$$z_i = \sqrt{a_i} y_i.$$

Equivalently, if $M_m(a)$ is the common-value coordinate matrix and D is the diagonal matrix with entries 1 on spine coordinates and $\sqrt{a_i}$ on the pendant coordinate at v_i , then

$$Q_m(a) = DM_m(a)D^{-1}.$$

In the orthonormal basis consisting of the spine edges and the vectors u_i , the restricted matrix becomes a real symmetric matrix $Q_m(a)$, and the eigenvalue equations take the form

$$\lambda x_j = -\left(\frac{1}{d_j} + \frac{1}{d_{j+1}}\right)x_j + \frac{\mathbf{1}_{j>1}}{d_j}x_{j-1} + \frac{\mathbf{1}_{j<m-1}}{d_{j+1}}x_{j+1} + \frac{\sqrt{a_j}}{d_j}z_j + \frac{\sqrt{a_{j+1}}}{d_{j+1}}z_{j+1},$$

where the terms involving z_j or z_{j+1} are omitted when the corresponding a -entry is zero, and

$$\lambda z_i = \frac{\sqrt{a_i}}{d_i}(\mathbf{1}_{i>1}x_{i-1} + \mathbf{1}_{i<m}x_i) - \frac{q_i + 2}{d_i}z_i.$$

The matrices used in Sections 4 and 5 are always these symmetric orthonormal orbit matrices. This is the setting in which Schur complements and Sylvester's criterion apply directly.

We can now state the main classification theorems.

For caterpillar parameters of the same spine order, define the coordinatewise partial order by $a \leq b$ if $a_i \leq b_i$ for all i . Two parameters are said to be coordinatewise comparable if either $a \leq b$ or $b \leq a$. A subset \mathcal{A} of caterpillar parameters is called downward closed if $b \in \mathcal{A}$ and $a \leq b$ imply $a \in \mathcal{A}$, and upward closed if $a \in \mathcal{A}$ and $a \leq b$ imply $b \in \mathcal{A}$. For a subset \mathcal{A} of caterpillar parameters, an element $a \in \mathcal{A}$ is called maximal in \mathcal{A} if there is no $b \in \mathcal{A}$ with $a < b$.

Theorem 2.1 (Classification of positive-curvature trees). *Let T be a finite tree. Then the discrete Einstein metric on T has positive curvature if and only if $\lambda_{\max}(R_T) < 0$. Such a tree must be a caterpillar. More precisely, the negative region of caterpillars is as follows.*

(i) For $m = 1$, i.e. for stars S_k , every $k \geq 1$ satisfies $\lambda_{\max}(R_{S_k}) < 0$.

(ii) For $m = 2$, i.e. for double stars $T_2(a_1, a_2)$,

$$\lambda_{\max}(R_{T_2(a_1, a_2)}) < 0 \iff (a_1 - 1)(a_2 - 1) < 4.$$

(iii) For $3 \leq m \leq 11$, the negative region is the downward closure of the maximal elements listed in Table 1.

(iv) For $m \geq 12$,

$$\lambda_{\max}(R_{T_m(a)}) < 0$$

if and only if

$$a = (a_1, 0, \dots, 0, a_m), \quad 1 \leq a_1, a_m \leq 3, \quad (a_1, a_m) \neq (3, 3).$$

Theorem 2.2 (The zero level set). *Among non-caterpillar trees with $\lambda_{\max}(R_T) = 0$, the only example is S_3^2 . Every tree that properly contains S_3^2 as a connected subtree has $\lambda_{\max}(R_T) > 0$. Among caterpillars, the zero level set consists of the stable family*

$$(3, 0, \dots, 0, 3),$$

obtained by subdividing the central edge of the double star $S_{3,3}$, together with the finite list in Table 2, up to reversal.

Remark 2.2. The proof separates the structural reductions from the finite verification. The stable zero family $(3, 0, \dots, 0, 3)$ already appears in [24, Proposition 8]; the new point here is the complete exhaustion of both the negative region and the zero level set.

3 Preliminary Reductions

This section collects the preliminary reductions used throughout the classification. The main ingredient is a Rayleigh-quotient argument for leaf attachment, based on a useful vertex decomposition of the Ricci matrix.

For an edge function $f : E(T) \rightarrow \mathbb{R}$, put

$$S_v(f) = \sum_{e \ni v} f_e, \quad A_v(f) = \sum_{e \ni v} f_e^2.$$

A direct expansion of the definition of R_T gives the vertex decomposition

$$\langle f, R_T f \rangle = \sum_{v \in V(T)} \frac{1}{d_v} (S_v(f)^2 - 2A_v(f)).$$

Indeed, at a fixed vertex v ,

$$2 \sum_{\{e, e'\} \subset E_v} f_e f_{e'} = \left(\sum_{e \in E_v} f_e \right)^2 - \sum_{e \in E_v} f_e^2,$$

and combining this with the diagonal contribution yields the displayed formula.

Once the implication

$$\lambda_{\max}(R_T) < 0 \implies T \text{ is a caterpillar}$$

is known, the non-caterpillar sign consequences can be recovered after the present classification is established. Moreover, in view of the leaf-attachment monotonicity established in the previous paper, compare [24, Propositions 3 and 7], the following conclusion may also be derived from the earlier results. We nevertheless record an independent Rayleigh-quotient proof, both for completeness and because it is the form used later in the zero-layer argument.

Proposition 3.1 (Monotonicity of the nonnegative region under leaf attachment). *Let T' be obtained from T by attaching one pendant edge at a vertex v . If*

$$\lambda_{\max}(R_T) \geq 0,$$

then

$$\lambda_{\max}(R_{T'}) \geq 0.$$

Moreover, if $\lambda_{\max}(R_T) > 0$, then $\lambda_{\max}(R_{T'}) > 0$.

Proof. Let $d = d_v$. Extend an old edge function f to T' by assigning value y to the new pendant edge. Only the local contribution at v and the new leaf endpoint changes. Put

$$S = \sum_{e \ni v} f_e, \quad A = \sum_{e \ni v} f_e^2.$$

Then

$$\begin{aligned} \Delta(y) &= \langle \tilde{f}, R_{T'} \tilde{f} \rangle - \langle f, R_T f \rangle \\ &= -\frac{S^2 - 2A}{d(d+1)} + \frac{2Sy}{d+1} - \frac{d+2}{d+1} y^2. \end{aligned}$$

This quadratic polynomial is maximized at $y = S/(d+2)$, and

$$\max_y \Delta(y) = \frac{2}{d(d+1)} \left(A - \frac{S^2}{d+2} \right) \geq 0$$

by Cauchy's inequality. If R_T has a nonnegative Rayleigh quotient, the extended vector can be chosen so that

$$\langle \tilde{f}, R_{T'} \tilde{f} \rangle \geq \langle f, R_T f \rangle.$$

Hence, if $\langle f, R_T f \rangle \geq 0$, the extension can be chosen so that $\langle \tilde{f}, R_{T'} \tilde{f} \rangle \geq 0$. Since $\|\tilde{f}\|^2 > 0$, this gives a nonnegative Rayleigh quotient for $R_{T'}$. If the original Rayleigh quotient is strictly positive, the same argument yields a strictly positive Rayleigh quotient for $R_{T'}$. \square

Corollary 3.1 (Strict crossing of the zero level set). *Let T' be obtained from T by attaching one pendant edge at an arbitrary vertex of T . If $\lambda_{\max}(R_T) = 0$, then*

$$\lambda_{\max}(R_{T'}) > 0.$$

Proof. Take the strictly positive Perron vector f of R_T . Then $A > 0$ and $S^2 \leq dA < (d+2)A$, so

$$A - \frac{S^2}{d+2} > 0.$$

Therefore

$$\max_y \Delta(y) = \frac{2}{d(d+1)} \left(A - \frac{S^2}{d+2} \right) > 0.$$

Since $\langle f, R_T f \rangle = 0$, the corresponding extension has strictly positive Rayleigh quotient for $R_{T'}$, and hence

$$\lambda_{\max}(R_{T'}) > 0.$$

□

Example 3.1 (Stars). Let S_k be the star with k edges. Then

$$R_{S_k} = - \left(1 + \frac{2}{k} \right) I + \frac{1}{k} J,$$

where J is the $k \times k$ all-ones matrix. Hence

$$\lambda_{\max}(R_{S_k}) = -\frac{2}{k},$$

with Perron eigenvector $\mathbf{1}$.

Each edge of S_k joins the central vertex of degree k to a leaf of degree 1. Hence each diagonal entry of R_{S_k} is

$$-1 - \frac{1}{k},$$

and two distinct edges meet only at the center, contributing $1/k$ to the off-diagonal entry. Therefore $R_{S_k} = -(1 + 2/k)I + J/k$. The vector $\mathbf{1}$ is an eigenvector with eigenvalue

$$-1 - \frac{1}{k} + \frac{k-1}{k} = -\frac{2}{k}.$$

Example 3.2 (Double stars [24, Example 2]). Let $T_2(a, b)$ be the double star whose two spine vertices carry a and b pendant edges. Then

$$\lambda_{\max}(R_{T_2(a,b)}) < 0 \iff (a-1)(b-1) < 4,$$

and equality holds exactly when $(a-1)(b-1) = 4$.

In particular, up to symmetry, the zero cases are

$$(a, b) = (3, 3), (2, 5).$$

The symmetric case $(3, 3)$ will later generate the stable zero family

$$(3, 0, \dots, 0, 3)$$

by subdividing the central edge.

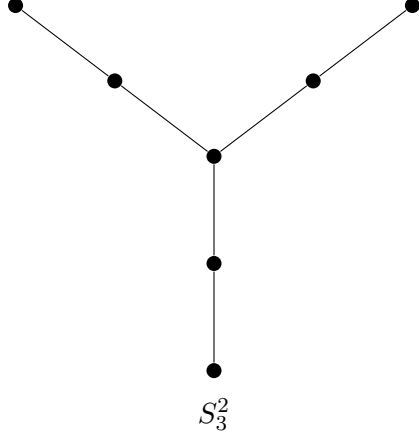


Figure 2: The unique non-caterpillar tree in the zero level set, namely S_3^2 .

3.1 Non-caterpillar reduction

Lemma 3.1. *Every non-caterpillar tree contains S_3^2 as a connected subtree.*

Proof. Let T° be the graph obtained from T by deleting all leaves. Since T is not a caterpillar, the graph T° is not a path. Therefore T° contains a vertex v of degree at least three. Choose three distinct neighbors u_1, u_2, u_3 of v in T° . Because each u_j still belongs to T° , it has a neighbor $w_j \neq v$ in T . The edges

$$vu_1, vu_2, vu_3, u_1w_1, u_2w_2, u_3w_3$$

form a connected subtree isomorphic to S_3^2 . □

Proposition 3.2 (The non-caterpillar part of the zero level set). *Let T be a non-caterpillar tree. Then*

$$\lambda_{\max}(R_T) = 0 \iff T = S_3^2.$$

In particular, if $T \neq S_3^2$, then $\lambda_{\max}(R_T) > 0$.

Proof. The equality $\lambda_{\max}(R_{S_3^2}) = 0$ is already recorded in [24, Definition 5 and the discussion preceding Proposition 4]. Equivalently, that paper gives a positive zero vector on S_3^2 with value 3 on the three edges incident to the center and value 1 on the three leaf edges. Hence $R_{S_3^2}w = 0$, and Perron–Frobenius implies that $\lambda_{\max}(R_{S_3^2}) = 0$. By Lemma 3.1, every non-caterpillar tree $T \neq S_3^2$ properly contains S_3^2 as a connected subtree. Since every finite tree can be obtained from any connected subtree by successively attaching pendant edges, there exists a finite sequence of trees

$$S_3^2 = T_0 \subset T_1 \subset \dots \subset T_k = T$$

such that, for each $j = 1, \dots, k$, the tree T_j is obtained from T_{j-1} by attaching one pendant edge at some vertex. By Corollary 3.1,

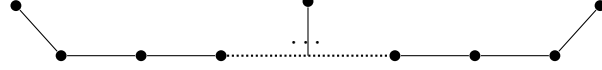
$$\lambda_{\max}(R_{T_1}) > 0.$$

Applying the strict part of Proposition 3.1 inductively along the sequence, we obtain

$$\lambda_{\max}(R_{T_j}) > 0, \quad 1 \leq j \leq k.$$

In particular,

$$\lambda_{\max}(R_T) > 0. \quad \square$$



$T_m(\eta_i)$: one pendant-edge orbit at v_1 , one at v_i , and one at v_m

Figure 3: The minimal internal defect $T_m(\eta_i)$.

4 Long-Spine Caterpillars

We now treat the case of long spines. The aim of this section is to show that, for $m \geq 12$, a caterpillar with $\lambda_{\max}(R_T) < 0$ cannot have any internal pendant edges. Once this has been proved, only the endpoint families $C_m(a, b)$ remain.

For a caterpillar, the pendant edges attached to a fixed spine vertex form a single orbit under the automorphism group permuting these sibling leaves. Because the Perron eigenvector is unique and positive, it is constant on each such orbit. Hence the spectral top $\lambda_{\max}(R_T)$ is equal to the spectral top of the symmetric orbit quotient introduced in Section 2.

To exclude internal pendant edges, we begin with the minimal configuration in which such a defect occurs. For each $2 \leq i \leq m - 1$, define

$$\eta_i = (1, 0, \dots, 0, \underset{i\text{-th position}}{1}, 0, \dots, 0, 1).$$

Thus the corresponding caterpillar $T_m(\eta_i)$ has exactly three pendant-edge orbits: one at each endpoint v_1, v_m , and one at the internal spine vertex v_i . Any caterpillar with an internal pendant edge at v_i is coordinatewise larger than this minimal defect.

The proof strategy for the long-spine case is therefore:

- (1) show that each minimal internal defect $T_m(\eta_i)$ already has

$$\lambda_{\max}(R_{T_m(\eta_i)}) \geq 0$$

when $m \geq 12$;

- (2) use the upward closure of the nonnegative region to exclude every caterpillar that contains an internal defect;
- (3) reduce the classification to the endpoint families $C_m(a, b)$.

Lemma 4.1 (Schur determinant for one internal pendant edge). *Let $m \geq 4$ and $2 \leq i \leq m - 1$, and let $Q_{m,i}$ be the equivariant quotient matrix for the caterpillar $T_m(\eta_i)$ in the orthonormal orbit basis of Section 2. Equivalently, $Q_{m,i}$ is obtained from the symmetric quotient matrix $Q_m(a)$ by specializing the parameter vector to η_i . Order the quotient variables by first listing the $m - 1$ spine-edge variables and then the three pendant-edge orbit variables at v_1, v_i, v_m . After eliminating these three pendant-edge variables, let $S_{m,i}$ denote the Schur complement on the spine-edge variables. Then*

$$\det S_{m,i} = (-1)^{m+1} \frac{B_{m,i}}{81 \cdot 2^{m-2}},$$

where

$$B_{m,i} = 8i^2 - 8im - 8i + 13m + 20.$$

If $B_{m,i} \leq 0$, then $\lambda_{\max}(Q_{m,i}) \geq 0$. If $B_{m,i} < 0$, then $\lambda_{\max}(Q_{m,i}) > 0$.

The determinant identity in Lemma 4.1 is also checked by the symbolic validation script described in Appendix C.

Proof. With the variable ordering specified above, the quotient matrix has the block form

$$Q_{m,i} = \begin{pmatrix} A & C \\ C^\top & D \end{pmatrix},$$

where A is the spine-edge block and D is the 3×3 block indexed by the three pendant-edge orbit variables. The pendant block is

$$D = \text{diag} \left(-\frac{3}{2}, -\frac{4}{3}, -\frac{3}{2} \right),$$

which is negative definite. The Schur complement of D in $Q_{m,i}$ is

$$S_{m,i} = A - CD^{-1}C^\top = A + \frac{1}{6}e_1e_1^\top + \frac{1}{12}(e_{i-1} + e_i)(e_{i-1} + e_i)^\top + \frac{1}{6}e_{m-1}e_{m-1}^\top,$$

where e_1, \dots, e_{m-1} are the standard basis vectors of \mathbb{R}^{m-1} . Here the eliminated block D belongs to the three orbit variables at v_1, v_i, v_m , not to the full individual pendant-edge basis. The matrix A is the tridiagonal spine block coming from the general quotient system. Away from the internal defect, the diagonal entries are -1 and the off-diagonal entries are $1/2$. At the defect one has

$$(S_{m,i})_{i-1,i-1} = (S_{m,i})_{i,i} = -\frac{3}{4}, \quad (S_{m,i})_{i-1,i} = (S_{m,i})_{i,i-1} = \frac{5}{12},$$

and the two endpoints have diagonal entry $-5/6$. When $i = 2$ or $i = m - 1$, the endpoint correction overlaps with one of the defect rows. In the case $i = 2$, the first two principal minors are obtained directly from the displayed Schur-complement formula:

$$P_1 = -\frac{7}{12}, \quad P_2 = \frac{19}{72},$$

which agree with the formulas for P_{i-1} and P_i below after specializing $i = 2$; from $k = 3$ onward, the tridiagonal coefficients are the same as in the generic case until the final endpoint row. The case $i = m - 1$ is the left-right reflection of $i = 2$ and gives the same initial values at the right end.

Let P_k be the leading k -th principal minor of $S_{m,i}$. The tridiagonal recurrence is

$$P_k = \alpha_k P_{k-1} - \beta_{k-1}^2 P_{k-2}, \quad P_0 = 1,$$

where α_k is the k -th diagonal entry and β_k the k -th off-diagonal entry. Before the defect,

$$P_k = (-1)^k \frac{2k+3}{3 \cdot 2^k}, \quad 0 \leq k \leq i-2.$$

Passing through the two defect rows gives

$$P_{i-1} = (-1)^{i-1} \frac{2i+3}{3 \cdot 2^i}, \quad P_i = (-1)^i \frac{2i+53}{54 \cdot 2^i}.$$

To the right of the defect the recurrence again becomes $P_k = -P_{k-1} - P_{k-2}/4$. Writing

$$U_k := (-1)^k 2^k P_k,$$

this becomes

$$U_k = 2U_{k-1} - U_{k-2},$$

whose characteristic polynomial $(r - 1)^2$ has a double root at $r = 1$. Hence U_k is affine in k , say $U_k = A_0 + B_0k$, and therefore

$$P_k = \frac{(-1)^k}{2^k}(A_0 + B_0k), \quad i \leq k \leq m - 2,$$

with

$$A_0 = \frac{16i^2 - 24i + 53}{54}, \quad B_0 = \frac{13 - 8i}{27}.$$

These constants are determined by the two initial values P_{i-1} and P_i . The final endpoint row has diagonal entry $-5/6$, and substitution gives

$$P_{m-1} = (-1)^{m+1} \frac{8i^2 - 8im - 8i + 13m + 20}{81 \cdot 2^{m-2}}.$$

This is the displayed determinant formula. By the inertia formula,

$$\text{In}(Q_{m,i}) = \text{In}(D) + \text{In}(S_{m,i}).$$

Here $\text{In}(M)$ denotes the inertia of a real symmetric matrix M , namely the triple consisting of the numbers of positive, negative, and zero eigenvalues. Since D is negative definite, the matrix $Q_{m,i}$ has a nonnegative eigenvalue as soon as $S_{m,i}$ is not negative definite. Now, if $S_{m,i}$ were negative definite, the sign of its determinant would be $(-1)^{m-1}$. When $B_{m,i} \leq 0$, the determinant is zero or has the opposite sign, so $S_{m,i}$ is not negative definite. Hence $Q_{m,i}$ has a nonnegative eigenvalue. If $B_{m,i} < 0$, then $\det S_{m,i} \neq 0$, hence also $\det Q_{m,i} \neq 0$ because D is invertible. Therefore 0 is not an eigenvalue of $Q_{m,i}$, and the already obtained nonnegative eigenvalue is in fact strictly positive. \square

Corollary 4.1. *Let $m \geq 12$, and let $T_m(a)$ be a caterpillar. If*

$$\lambda_{\max}(R_{T_m(a)}) < 0,$$

then

$$a_i = 0, \quad 2 \leq i \leq m - 1.$$

Proof. For $2 \leq i \leq m - 1$, the quadratic polynomial

$$B_{m,i} = 8i^2 - 8im - 8i + 13m + 20$$

is convex in i , hence attains its maximum on the interval

$$2 \leq i \leq m - 1$$

at one of the two endpoints. A direct computation gives

$$B_{m,2} = 36 - 3m, \quad B_{m,m-1} = 36 - 3m,$$

and therefore

$$B_{m,i} \leq 0, \quad 2 \leq i \leq m - 1,$$

for every $m \geq 12$. By Lemma 4.1, each minimal internal defect $T_m(\eta_i)$ then satisfies

$$\lambda_{\max}(R_{T_m(\eta_i)}) \geq 0.$$

Finally, Proposition 3.1 implies that the nonnegative region is upward closed. Hence every caterpillar containing an internal defect is also nonnegative. Therefore a caterpillar with

$$\lambda_{\max}(R_{T_m(a)}) < 0$$

cannot have any internal pendant edge, that is,

$$a_i = 0, \quad 2 \leq i \leq m - 1.$$

□

Corollary 4.2 (Long-spine zero-layer reduction). *Let $m \geq 13$, and let $T_m(a)$ be a caterpillar. If $a_i > 0$ for some $2 \leq i \leq m - 1$, then*

$$\lambda_{\max}(R_{T_m(a)}) > 0.$$

Consequently, every caterpillar with $m \geq 13$ and $\lambda_{\max}(R_{T_m(a)}) \leq 0$ is endpoint-only.

Proof. If $a_i > 0$ for some internal index i , then $T_m(a)$ contains the minimal internal defect $T_m(\eta_i)$. For $m \geq 13$, the endpoint computation above gives $B_{m,i} \leq 36 - 3m < 0$, so Lemma 4.1 yields

$$\lambda_{\max}(R_{T_m(\eta_i)}) > 0.$$

Applying the strict part of Proposition 3.1 along any sequence of leaf attachments from $T_m(\eta_i)$ to $T_m(a)$ gives

$$\lambda_{\max}(R_{T_m(a)}) > 0.$$

The final assertion is immediate. □

4.1 Endpoint families

Proposition 4.1 (Endpoint-only families). *Let*

$$C_m(a, b) = T_m(a, 0, \dots, 0, b).$$

For $m \geq 12$,

$$\lambda_{\max}(R_{C_m(a,b)}) < 0 \iff 1 \leq a, b \leq 3, \quad (a, b) \neq (3, 3).$$

Moreover, $C_m(3, 3)$ satisfies $\lambda_{\max}(R_{C_m(3,3)}) = 0$ for every $m \geq 2$.

Proof. We prove the assertion directly from the caterpillar quotient system in Section 2, specialized to the endpoint-only parameter vector

$$(a, 0, \dots, 0, b).$$

At energy $\lambda = 0$, we eliminate the two endpoint pendant-edge orbit variables and study the resulting Schur complement on the spine-edge variables. Let $n = m - 1$ be the number of spine edges. In the symmetric orbit quotient, the two eliminated endpoint orbit variables have diagonal entries $-3/(a + 1)$ and $-3/(b + 1)$, so the eliminated block is negative definite. The sibling-difference directions in the full edge space have eigenvalues $-(a + 3)/(a + 1)$ and $-(b + 3)/(b + 1)$, respectively, and are already negative; hence they do not affect the spectral top.

The Schur complement on the spine-edge variables is the tridiagonal matrix $S_n(a, b)$ with off-diagonal entries $1/2$, interior diagonal entries -1 , and endpoint diagonal entries

$$\alpha_a = -\frac{a+9}{6(a+1)}, \quad \alpha_b = -\frac{b+9}{6(b+1)}.$$

Thus $C_m(a, b)$ has $\lambda_{\max}(R_{C_m(a,b)}) < 0$ if and only if $S_n(a, b)$ is negative definite.

Let P_k be the leading k -th principal minor of $S_n(a, b)$. For $1 \leq k \leq n-1$,

$$P_k = (-1)^k 2^{-k} r_k, \quad r_k = 1 + \frac{k}{3} \rho_a, \quad \rho_a = \frac{2(3-a)}{a+1}.$$

For the final minor,

$$P_n = (-1)^n 2^{-n} t_n, \quad t_n = \frac{1}{3} \left[\rho_a - \sigma_b \left(1 + \frac{n-1}{3} \rho_a \right) \right],$$

where

$$\sigma_b = \frac{2(b-3)}{b+1}.$$

These formulae follow from the recurrence $P_k = \alpha_k P_{k-1} - (1/2)^2 P_{k-2}$, with the last step using α_b instead of the interior diagonal -1 .

By Sylvester's criterion, $S_n(a, b)$ is negative definite if and only if $(-1)^k P_k > 0$ for all $1 \leq k \leq n$. Suppose $m \geq 12$, so $n-1 \geq 10$. If $a \geq 4$, then $\rho_a \leq -2/5$, and hence

$$r_{n-1} = 1 + \frac{n-1}{3} \rho_a \leq 1 - \frac{10}{3} \cdot \frac{2}{5} < 0,$$

so the matrix is not negative definite. By symmetry, the same conclusion holds if $b \geq 4$.

It remains to consider $1 \leq a, b \leq 3$. Then $\rho_a \geq 0$ and $\sigma_b \leq 0$, so every r_k is positive and $t_n > 0$ unless $\rho_a = \sigma_b = 0$, which is precisely $(a, b) = (3, 3)$. Hence all these endpoint families are negative except $(3, 3)$.

For $(a, b) = (3, 3)$, the eliminated spine matrix has endpoint diagonals $-1/2$, interior diagonals -1 , and off-diagonals $1/2$. The constant spine vector lies in its kernel. Equivalently, in the original tree, putting the spine-edge weights equal to 3 and all pendant-edge weights equal to 1 gives $R_T w = 0$. Since $w > 0$, Perron–Frobenius gives $\lambda_{\max}(R_T) = 0$. \square

Corollary 4.3 (Long-spine zero endpoint family). *Let $m \geq 13$. Among endpoint-only caterpillars $C_m(a, b)$, one has*

$$\lambda_{\max}(R_{C_m(a,b)}) = 0 \iff (a, b) = (3, 3).$$

Equivalently, among endpoint-only caterpillars with $m \geq 13$, the zero level set consists exactly of the family $(3, 0, \dots, 0, 3)$.

Proof. Let $n = m-1 \geq 12$ and let $S_n(a, b)$ be the Schur complement from the proof of Proposition 4.1. If

$$\lambda_{\max}(R_{C_m(a,b)}) = 0,$$

then the symmetric orbit matrix $Q_m(a, b)$ is negative semidefinite. Since the eliminated endpoint blocks are negative definite, the Schur complement $S_n(a, b)$ is also negative semidefinite. Since every principal submatrix of a negative semidefinite matrix is again negative semidefinite, each leading principal submatrix of $S_n(a, b)$ has determinant P_k , and therefore

$$(-1)^k P_k \geq 0, \quad 1 \leq k \leq n.$$

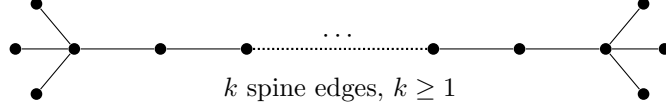


Figure 4: The stable zero-eigenvalue family $(3, 0, \dots, 0, 3)$, obtained by subdividing the central edge of the double star $S_{3,3}$.

Suppose first that $a \geq 4$. Then $\rho_a \leq -2/5$, so

$$r_{n-1} = 1 + \frac{n-1}{3}\rho_a \leq 1 - \frac{11}{3} \cdot \frac{2}{5} < 0$$

because $n-1 \geq 11$. Hence

$$(-1)^{n-1}P_{n-1} = 2^{-(n-1)}r_{n-1} < 0,$$

contrary to negative semidefiniteness. By symmetry, one also cannot have $b \geq 4$. Thus any endpoint-only zero example with $m \geq 13$ must satisfy $1 \leq a, b \leq 3$.

For $1 \leq a, b \leq 3$, Proposition 4.1 already shows that every family other than $(a, b) = (3, 3)$ is strictly negative, while $(3, 3)$ has zero largest eigenvalue. Therefore

$$\lambda_{\max}(R_{C_m(a,b)}) = 0 \iff (a, b) = (3, 3).$$

□

For long spines, Corollary 4.1 leaves only these endpoint families. Proposition 4.1 therefore gives the stable zero-eigenvalue family

$$(3, 0, \dots, 0, 3).$$

Remark 4.1. Once the zero-eigenvalue family $(3, 0, \dots, 0, 3)$ is known, Proposition 3.1 and Corollary 3.1 already determine the sign of all endpoint families that are coordinatewise comparable with it. However, this does not cover the whole endpoint region, because families such as $C_m(4, 1)$ or $C_m(5, 3)$ are not coordinatewise comparable with $C_m(3, 3)$. For this reason, Proposition 4.1 cannot be replaced by a direct corollary of the zero-eigenvalue family and requires the Schur-complement analysis above.

Together with Corollary 4.1, this proves the long-spine part of Theorem 2.1.

5 Short-Spine Verification

After the separate treatments of $m = 1$, $m = 2$, and $m \geq 12$, the only remaining range is $3 \leq m \leq 11$. In this finite regime, downward closure reduces the problem to the maximal negative elements. They are listed in Table 1. The $m = 12$ row is included as the first instance of the long-spine endpoint rule and as a consistency check for the finite enumeration.

More explicitly, for a fixed spine order m let

$$\mathcal{N}_m = \{a : \lambda_{\max}(R_{T_m(a)}) < 0\}.$$

Proposition 3.1 says that the complement of \mathcal{N}_m is upward closed, and therefore \mathcal{N}_m is downward closed. Hence the finite table is organized by the maximal elements of \mathcal{N}_m with respect to the

coordinatewise partial order: once these are known, the whole negative region is exactly their coordinatewise downward closure. To determine the zero level set, we also look at the first nonnegative boundary

$$\partial_+ \mathcal{N}_m = \{a \notin \mathcal{N}_m : \text{every immediate predecessor of } a \text{ lies in } \mathcal{N}_m\}$$

in the same finite range. This boundary is listed in Appendix A.

The finite verification is carried out by the deterministic procedure below. Here \bar{a} denotes the canonical representative of a up to reversal.

- (1) Start from the minimal canonical parameter

$$a^{(0)} = (1, 0, \dots, 0, 1).$$

- (2) For every parameter a reached by the search, compute the sign of $\lambda_{\max}(R_{T_m(a)})$.
- (3) If $\lambda_{\max}(R_{T_m(a)}) < 0$, record a as negative and add all canonical children

$$\overline{a + e_i}, \quad 1 \leq i \leq m,$$

to the search queue.

- (4) If $\lambda_{\max}(R_{T_m(a)}) \geq 0$, stop in that direction; by Proposition 3.1, every coordinatewise larger parameter is also nonnegative.

Since \mathcal{N}_m is downward closed, every negative parameter is reached by this procedure: along any coordinatewise path from $(1, 0, \dots, 0, 1)$ to a negative parameter, all intermediate parameters are also negative. When the procedure terminates, the recorded negative parameters with no negative child are exactly the maximal elements of \mathcal{N}_m .

For a fixed caterpillar parameter a , the restricted operator from Section 2 has rational entries in the coordinate basis (x_j, y_i) . The symmetric orthonormal orbit matrix $Q_m(a)$ from Section 2 is obtained from this coordinate matrix by a positive diagonal similarity, so both matrices have the same spectrum. Concretely, if $M_m(a)$ denotes the common-value coordinate matrix and D is diagonal with entries 1 on the spine coordinates and $\sqrt{a_i}$ on each pendant-orbit coordinate corresponding to a vertex with $a_i > 0$, then

$$Q_m(a) = DM_m(a)D^{-1}.$$

The remaining eigenspaces come from differences of sibling pendant edges and have negative eigenvalues. Hence the inequality

$$\lambda_{\max}(R_{T_m(a)}) < 0$$

is equivalent to negative definiteness of the symmetric orbit matrix $Q_m(a)$. For the finite verification we instead use an exact rational computation on the coordinate matrix of this restricted operator. For each parameter a , we form the characteristic polynomial over \mathbb{Q} , determine the multiplicity of the root $\lambda = 0$, and use Sturm root counts to count the roots in the positive half-line $(0, \infty)$. ThusThus

$$\lambda_{\max}(R_{T_m(a)}) < 0 \iff 0 \text{ is not a root of } \chi_a \text{ and } \chi_a \text{ has no root in } (0, \infty),$$

$$\lambda_{\max}(R_{T_m(a)}) = 0 \iff 0 \text{ is a root of } \chi_a \text{ and } \chi_a \text{ has no root in } (0, \infty),$$

and

$$\lambda_{\max}(R_{T_m(a)}) > 0 \iff \chi_a \text{ has a root in } (0, \infty).$$

m	Maximal negative elements
3	(1, 1, 2), (1, 3, 1), (2, 0, 4), (1, 0, 8)
4	(1, 0, 2, 1), (1, 1, 0, 2), (1, 0, 0, 5), (2, 0, 0, 4)
5	(1, 0, 1, 0, 1), (1, 1, 0, 0, 2), (1, 0, 0, 0, 4), (2, 0, 0, 0, 3)
6	(1, 0, 0, 1, 0, 1), (1, 1, 0, 0, 0, 2), (1, 0, 0, 0, 0, 4), (2, 0, 0, 0, 0, 3)
7	(1, 1, 0, 0, 0, 0, 2), (1, 0, 0, 0, 0, 0, 4), (2, 0, 0, 0, 0, 0, 3)
8	(1, 1, 0, 0, 0, 0, 0, 2), (2, 0, 0, 0, 0, 0, 0, 3)
9	(1, 0, 0, 0, 0, 0, 0, 1, 1), (2, 0, 0, 0, 0, 0, 0, 0, 3)
10	(1, 0, 0, 0, 0, 0, 0, 0, 1, 1), (2, 0, 0, 0, 0, 0, 0, 0, 0, 3)
11	(1, 0, 0, 0, 0, 0, 0, 0, 0, 1, 1), (2, 0, 0, 0, 0, 0, 0, 0, 0, 0, 3)
12	(2, 0, 0, 0, 0, 0, 0, 0, 0, 0, 3)

Table 1: Maximal elements of the negative caterpillar downsets. Each listed parameter satisfies $\lambda_{\max} < 0$, whereas increasing any single coordinate yields $\lambda_{\max} \geq 0$. For $3 \leq m \leq 11$, the full negative region is the coordinatewise downward closure of these maximal elements; the $m = 12$ row matches the long-spine classification.

m	Exceptional caterpillar zero parameters
2	(2, 5)
3	(1, 4, 1), (1, 0, 9)
4	(1, 0, 0, 6)
5	(2, 0, 0, 0, 4), (1, 0, 0, 0, 5)
8	(1, 0, 0, 0, 0, 0, 4)
9	(1, 1, 0, 0, 0, 0, 0, 2)
12	(1, 0, 0, 0, 0, 0, 0, 0, 0, 1, 1)

Table 2: Finite exceptional caterpillars in the zero level set. Together with the stable family $(3, 0, \dots, 0, 3)$, they exhaust all caterpillars with $\lambda_{\max}(R_T) = 0$.

These alternatives are therefore decided exactly by the zero multiplicity at $\lambda = 0$ together with the Sturm root count on $(0, \infty)$. Thus, for each entry a in Table 1, we check two finite conditions:

$$\lambda_{\max}(R_{T_m(a)}) < 0,$$

and, for every $1 \leq i \leq m$,

$$\lambda_{\max}(R_{T_m(\overline{a+e_i})}) \geq 0.$$

The first condition says that a lies in the negative region; the second says that it is maximal in that region. The same exact rational sign computation is used for the first nonnegative boundary. The entries in Table 2 have explicit positive null vectors, listed in Appendix B.1. Since these null vectors are strictly positive, Perron–Frobenius implies that the corresponding zero eigenvalue is the largest eigenvalue. The other boundary points in Appendix A have strictly positive largest eigenvalue.

Thus the finite verification is exact and reproducible. It uses exact rational arithmetic and Sturm root counts rather than floating-point tests, together with the monotonicity theorem as the stopping rule. Every child

$$\overline{a + e_i}$$

is checked explicitly by an exact rational computation on the quotient matrix. The verification code and output files are described in Appendix C.

5.1 Zero examples

After the long-spine analysis, only the short spines

$$3 \leq m \leq 12$$

must be checked. In this range, Proposition 3.1 controls the search space, so the negative region is determined by the maximal elements in Table 1, while the zero classification is read off from the first nonnegative boundary recorded in Appendix A. Indeed, if an immediate predecessor of a zero parameter were nonnegative, then adding the corresponding leaf would make the new parameter strictly positive by Proposition 3.1 and Corollary 3.1, contradicting $\lambda_{\max} = 0$.

The double-star family gives an illustrative model for the phase transition. By Example 3.2, the sign is governed by the single threshold

$$\lambda_{\max}(R_{T_2(a,b)}) < 0 \iff (a-1)(b-1) < 4,$$

with equality

$$\lambda_{\max}(R_{T_2(a,b)}) = 0 \iff (a-1)(b-1) = 4.$$

Thus the zero-eigenvalue points are

$$(a, b) = (3, 3), (2, 5), (5, 2),$$

up to the symmetry interchanging the two ends. This is the first appearance of the stable family: subdividing the central edge of $(3, 3)$ gives the zero caterpillars

$$(3, 0, \dots, 0, 3).$$

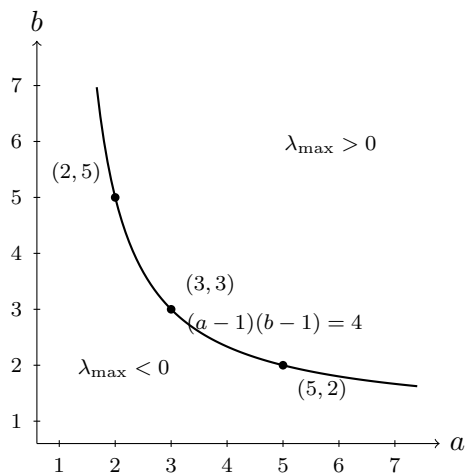


Figure 5: Phase diagram for the double-star family $T_2(a, b)$. The curve $(a-1)(b-1) = 4$ separates the negative and positive regions, and the marked lattice points are exactly the zero cases.

These examples also show that symmetry alone is not the correct organizing principle for λ_{\max} . The symmetric double star $(3, 3)$ lies in the zero level set, whereas highly asymmetric double stars such as

$$(1, n-3)$$

still remain in the negative region.

For the zero level set, the long-spine part is already settled by Corollaries 4.2 and 4.3, so every remaining zero caterpillar must lie in the finite range $m \leq 12$. Corollary 3.1 places such cases on the first nonnegative boundary, and the exact verification shows that the zero points there are precisely those in Table 2. Therefore the zero level set consists of the stable family $(3, 0, \dots, 0, 3)$, the nine exceptional short-spine caterpillars, and the single non-caterpillar tree S_3^2 .

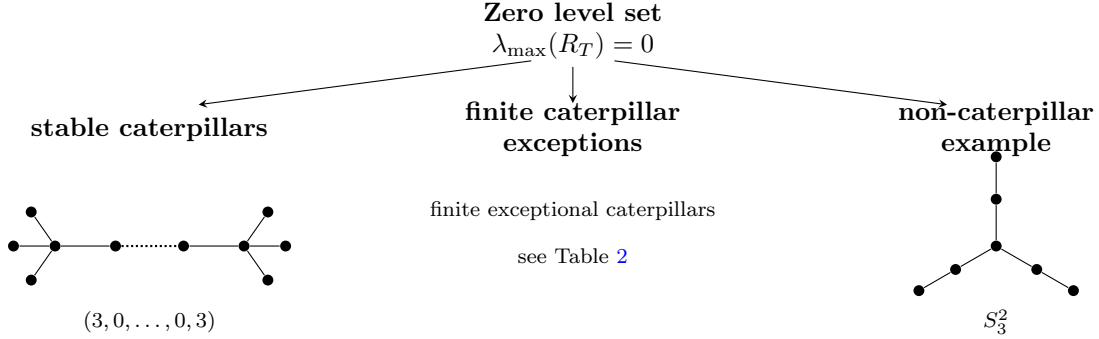


Figure 6: Schematic structure of the zero level set. Its caterpillar part consists of the stable family $(3, 0, \dots, 0, 3)$ together with the nine finite exceptional parameters in Table 2, while its non-caterpillar part consists only of S_3^2 .

6 Infinite Trees

The classification above is intrinsically finite. If T is an infinite locally finite tree, the matrix R_T should be interpreted as an operator on edge functions. When the degrees are uniformly bounded, it defines a bounded self-adjoint operator on $\ell^2(E(T))$. More generally, one can still consider the Rayleigh quotient on finitely supported edge functions and set

$$\Lambda_c(T) = \sup_{0 \neq f \in C_c(E(T))} \frac{\langle f, R_T f \rangle}{\langle f, f \rangle}.$$

Here $C_c(E(T))$ denotes the space of finitely supported real-valued functions on the edge set $E(T)$. For bounded-degree trees, $\Lambda_c(T) = \sup \sigma(R_T)$.

Proposition 6.1 (Infinite trees). *Let T be an infinite locally finite tree. Then*

$$\Lambda_c(T) \geq 0.$$

In particular, if R_T is a bounded self-adjoint operator on $\ell^2(E(T))$, then $\sup \sigma(R_T) \geq 0$.

Proof. Every infinite locally finite tree contains a one-sided infinite simple path

$$e_1, e_2, e_3, \dots$$

For $N \geq 1$, define $f_N(e_j) = 1$ for $1 \leq j \leq N$ and $f_N(e) = 0$ otherwise. By the vertex decomposition, every interior vertex of the selected path segment has exactly two incident selected edges, and therefore its local contribution is

$$\frac{1}{d_v}(2^2 - 2 \cdot 2) = 0.$$

Only the two endpoints of the segment contribute, and each endpoint contribution is bounded below by -1 . Hence

$$\langle f_N, R_T f_N \rangle \geq -2, \quad \|f_N\|^2 = N.$$

Therefore the Rayleigh quotients of f_N tend to 0 from below, and $\Lambda_c(T) \geq 0$. □

Remark 6.1 (Infinite trees). The proposition shows that no infinite locally finite tree has a negative spectral top in this sense. For example, the infinite path lies in the zero level set: its spectral top is 0. Finite positive-curvature trees can converge to the zero level set when the spine order tends to infinity; the stable finite family $(3, 0, \dots, 0, 3)$ is one such manifestation. The usual finite statement that a tree in the zero level set becomes positive after attaching a leaf uses a positive Perron eigenvector and does not directly apply to the edge of the essential spectrum on an infinite path. The half-line endpoint models $(a, 0, 0, \dots)$ therefore require a separate one-dimensional analysis.

Acknowledgements

The author is grateful to Bobo Hua for his support, and to Shuliang Bai for helpful discussions and suggestions.

References

- [1] A. L. Besse, *Einstein Manifolds*, Ergebnisse der Mathematik und ihrer Grenzgebiete (3), 10. Springer-Verlag, Berlin, 1987.
- [2] R. Hamilton, Three-manifolds with positive Ricci curvature, *J. Differential Geom.* **17** (1982), 255–306.
- [3] B. Chow, P. Lu, and L. Ni, *Hamilton’s Ricci Flow*, Graduate Studies in Mathematics, 77. American Mathematical Society, Providence, RI; Science Press, New York, 2006.
- [4] Y. Ollivier, Ricci curvature of Markov chains on metric spaces, *J. Funct. Anal.* **256** (2009), 810–864.
- [5] Y. Lin, L. Lu, and S.-T. Yau, Ricci curvature of graphs, *Tohoku Math. J.* **63** (2011), 605–627.
- [6] F. Bauer, J. Jost, and S. Liu, Ollivier-Ricci curvature and the spectrum of the normalized graph Laplace operator, *Math. Res. Lett.* **19** (2012), 1185–1205.
- [7] J. Jost and S. Liu, Ollivier’s Ricci curvature, local clustering and curvature-dimension inequalities on graphs, *Discrete Comput. Geom.* **51** (2014), 300–322.
- [8] Y. Lin and S.-T. Yau, Ricci curvature and eigenvalue estimate on locally finite graphs, *Math. Res. Lett.* **17** (2010), 343–356.
- [9] H.-J. Cho, S-H Paeng, Ollivier’s Ricci curvature and the coloring of graphs, *European J. Combin.* **34** (2013), no. 5, 916–922.
- [10] S.-H. Paeng, Volume and diameter of a graph and Ollivier’s Ricci curvature, *European J. Combin.* **33** (2012), 1808–1819.
- [11] D. Bourne, D. Cushing, S. Liu, F. Münch, and N. Peyerimhoff, Ollivier-Ricci idleness functions of graphs, *SIAM J. Discrete Math.* **32** (2018), no. 2, 1408–1424.

- [12] F. Münch and R. K. Wojciechowski, Ollivier Ricci curvature for general graph Laplacians: heat equation, Laplacian comparison, non-explosion and diameter bounds, *Adv. Math.* **356** (2019), 106759.
- [13] D. Cushing, S. Kamtue, R. Kangaslampi, S. Liu, and N. Peyerimhoff, Curvatures, graph products and Ricci flatness, *J. Graph Theory* **96** (2021), no. 4, 522–553.
- [14] D. Cushing, R. Kangaslampi, V. Lipiäinen, S. Liu, and G. W. Stagg, The graph curvature calculator and the curvatures of cubic graphs, *Exp. Math.* **31** (2022), no. 2, 583–595.
- [15] A. Samal, R. P. Sreejith, J. Gu, S. Liu, E. Saucan, and J. Jost, Comparative analysis of two discretizations of Ricci curvature for complex networks, *Sci. Rep.* **8** (2018), Article No. 8650.
- [16] J. Sia, E. Jonckheere, and P. Bogdan, Ollivier-Ricci curvature-based method to community detection in complex networks, *Sci. Rep.* **9** (2019), Article No. 9800.
- [17] A. Gosztolai and A. Arnaudon, Unfolding the multiscale structure of networks with dynamical Ollivier-Ricci curvature, *Nat. Commun.* **12** (2021), Article No. 4561.
- [18] P. van der Hoorn, G. Lippner, C. Trugenberger, and D. Krioukov, Ollivier curvature of random geometric graphs converges to Ricci curvature of their Riemannian manifolds, *Discrete Comput. Geom.* **70** (2023), no. 3, 671–712.
- [19] M. Hehl, Graphs with Lin-Lu-Yau curvature at least one and regular bone-idle graphs, *Calc. Var. Partial Differential Equations* **64** (2025), Article No. 196.
- [20] M. Hehl, Regular graphs with positive Ollivier–Ricci curvature, *Math. Ann.* **394** (2026), Article No. 24.
- [21] S. Bai, A. Huang, L. Lu, and S.-T. Yau, On the sum of Ricci curvatures for weighted graphs, *Pure Appl. Math. Q.* **17** (2021), 1599–1617.
- [22] S. Bai, Y. Lin, L. Lu, Z. Wang, and S.-T. Yau, Ollivier Ricci-flow on weighted graphs, *Amer. J. Math.* **146** (2024), 1033–1064.
- [23] S. Bai, B. Hua, Y. Lin, and S. Liu, *On the Ricci flow on trees*, preprint, arXiv:2509.22140, 2025.
- [24] S. Bai and B. Hua, *Discrete Einstein metrics on trees*, preprint, arXiv:2604.22449, 2026.
- [25] A. Berman and R. J. Plemmons, *Nonnegative Matrices in the Mathematical Sciences*, Academic Press, New York, 1979.

A Minimal Nonnegative Boundary

The following table records the minimal nonnegative boundary

$$\partial_+ \mathcal{N}_m$$

for

$$3 \leq m \leq 12.$$

Together with Table 1, it provides the exact finite data needed for the short-spine classification. Appendix B.1 then isolates the zero-eigenvalue entries from this boundary and records representative positive null vectors. A machine-readable version of this boundary table is included in the repository described in Appendix C.

m	Minimal nonnegative boundary
3	(1, 1, 3), (1, 2, 2), (2, 1, 2), (1, 4, 1), (3, 0, 3), (2, 0, 5), (1, 0, 9)
4	(1, 0, 1, 2), (1, 1, 1, 1), (1, 0, 3, 1), (1, 1, 0, 3), (1, 2, 0, 2), (3, 0, 0, 3), (1, 0, 0, 6), (2, 0, 0, 5)
5	(1, 0, 0, 1, 2), (1, 0, 0, 2, 1), (1, 0, 1, 0, 2), (1, 0, 1, 1, 1), (1, 0, 2, 0, 1), (1, 1, 0, 1, 1), (1, 1, 0, 0, 3), (1, 0, 0, 0, 5), (2, 0, 0, 0, 4), (3, 0, 0, 0, 3)
6	(1, 0, 0, 0, 1, 2), (1, 0, 0, 0, 2, 1), (1, 0, 0, 1, 0, 2), (1, 0, 0, 1, 1, 1), (1, 0, 0, 2, 0, 1), (1, 0, 1, 0, 0, 2), (1, 0, 1, 0, 1, 1), (1, 0, 1, 1, 0, 1), (1, 1, 0, 0, 1, 1), (1, 1, 0, 0, 0, 3), (1, 0, 0, 0, 0, 5), (2, 0, 0, 0, 0, 4), (3, 0, 0, 0, 0, 3)
7	(1, 0, 0, 0, 1, 0, 1), (1, 0, 0, 1, 0, 0, 1), (1, 0, 0, 0, 0, 1, 2), (1, 0, 0, 0, 0, 2, 1), (1, 1, 0, 0, 0, 1, 1), (1, 1, 0, 0, 0, 0, 3), (1, 0, 0, 0, 0, 0, 5), (2, 0, 0, 0, 0, 0, 4), (3, 0, 0, 0, 0, 0, 3)
8	(1, 0, 0, 0, 0, 1, 0, 1), (1, 0, 0, 0, 1, 0, 0, 1), (1, 0, 0, 0, 0, 0, 1, 2), (1, 0, 0, 0, 0, 0, 2, 1), (1, 1, 0, 0, 0, 0, 1, 1), (1, 0, 0, 0, 0, 0, 0, 4), (1, 1, 0, 0, 0, 0, 0, 3), (3, 0, 0, 0, 0, 0, 0, 3)
9	(1, 0, 0, 0, 0, 0, 1, 0, 1), (1, 0, 0, 0, 0, 1, 0, 0, 1), (1, 0, 0, 0, 1, 0, 0, 0, 1), (1, 0, 0, 0, 0, 0, 1, 2), (1, 0, 0, 0, 0, 0, 2, 1), (1, 1, 0, 0, 0, 0, 0, 0, 2), (1, 1, 0, 0, 0, 0, 0, 1, 1), (1, 0, 0, 0, 0, 0, 0, 0, 4), (3, 0, 0, 0, 0, 0, 0, 0, 3)
10	(1, 0, 0, 0, 0, 0, 1, 0, 1), (1, 0, 0, 0, 0, 0, 1, 0, 0, 1), (1, 0, 0, 0, 0, 1, 0, 0, 0, 1), (1, 0, 0, 0, 1, 0, 0, 0, 0, 1), (1, 0, 0, 0, 0, 0, 0, 0, 1, 2), (1, 0, 0, 0, 0, 0, 0, 0, 2, 1), (1, 1, 0, 0, 0, 0, 0, 0, 0, 2), (1, 1, 0, 0, 0, 0, 0, 0, 1, 1), (1, 0, 0, 0, 0, 0, 0, 0, 0, 4), (3, 0, 0, 0, 0, 0, 0, 0, 0, 3)
11	(1, 0, 0, 0, 0, 0, 0, 0, 1, 0, 1), (1, 0, 0, 0, 0, 0, 0, 1, 0, 0, 1), (1, 0, 0, 0, 0, 0, 1, 0, 0, 0, 1), (1, 0, 0, 0, 0, 1, 0, 0, 0, 0, 1), (1, 0, 0, 0, 1, 0, 0, 0, 0, 0, 1), (1, 0, 0, 0, 0, 0, 0, 0, 0, 1, 2), (1, 0, 0, 0, 0, 0, 0, 0, 0, 2, 1), (1, 1, 0, 0, 0, 0, 0, 0, 0, 0, 2), (1, 1, 0, 0, 0, 0, 0, 0, 0, 1, 1), (1, 0, 0, 0, 0, 0, 0, 0, 0, 0, 4), (3, 0, 0, 0, 0, 0, 0, 0, 0, 0, 3)
12	(1, 0, 0, 0, 0, 0, 0, 0, 0, 1, 1), (1, 0, 0, 0, 0, 0, 0, 0, 0, 1, 0, 1), (1, 0, 0, 0, 0, 0, 0, 0, 1, 0, 0, 1), (1, 0, 0, 0, 0, 0, 0, 0, 1, 0, 0, 0, 1), (1, 0, 0, 0, 0, 0, 1, 0, 0, 0, 0, 1), (1, 0, 0, 0, 0, 0, 0, 0, 0, 0, 0, 4), (3, 0, 0, 0, 0, 0, 0, 0, 0, 0, 0, 3)

B Zero Diagrams and Zero Vectors

The nine finite caterpillar zero exceptions from Table 2 are displayed below. In each diagram, the horizontal path is the spine, and the pendant edges are attached at the indicated spine vertices.

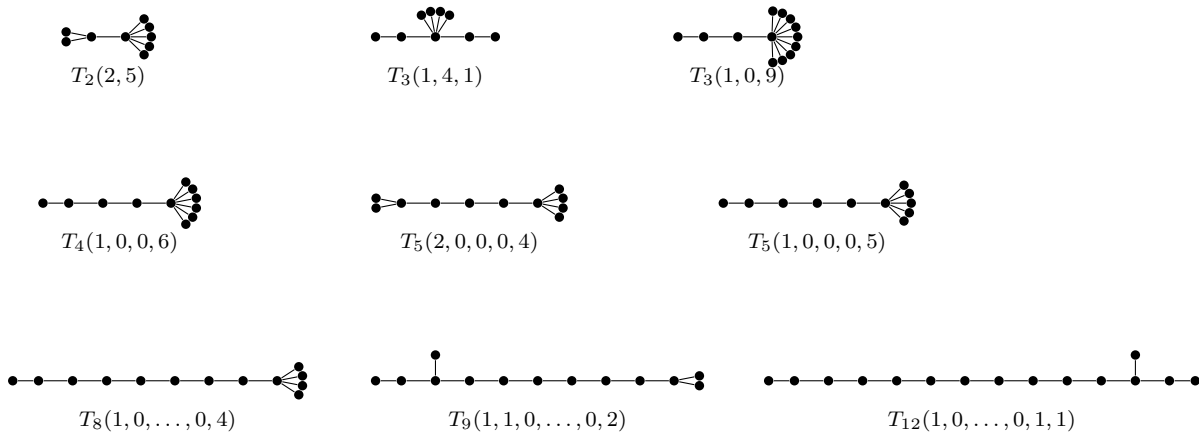


Figure 7: The nine finite caterpillar zero exceptions from Table 2.

B.1 Representative Zero Vectors

We use the following edge order: first list the spine edges

$$s_j = v_j v_{j+1}, \quad 1 \leq j \leq m-1,$$

and then list the pendant edges grouped by the spine vertices v_1, \dots, v_m . The following positive integer vectors satisfy

$$R_{T_m(a)} w = 0.$$

The first eight are listed in the table; the last one is displayed separately below for readability. By Perron–Frobenius, this zero eigenvalue is the largest eigenvalue. For example, in the row $(1, 4, 1)$, the two spine edges both have weight 6, the single leaf at each endpoint has weight 2, and the four leaves at the middle spine vertex all have weight 3.

a	spine-edge weights	pendant-edge weights, grouped by spine vertices
$(2, 5)$	(3)	$(1, 1) \mid (1, 1, 1, 1, 1)$
$(1, 4, 1)$	$(6, 6)$	$(2) \mid (3, 3, 3, 3) \mid (2)$
$(1, 0, 9)$	$(9, 15)$	$(3) \mid (5, 5, 5, 5, 5, 5, 5, 5)$
$(1, 0, 0, 6)$	$(9, 15, 21)$	$(3) \mid (7, 7, 7, 7, 7, 7)$
$(1, 0, 0, 0, 5)$	$(3, 5, 7, 9)$	$(1) \mid (3, 3, 3, 3, 3)$
$(2, 0, 0, 0, 4)$	$(9, 11, 13, 15)$	$(3, 3) \mid (5, 5, 5, 5)$
$(1, 0, 0, 0, 0, 0, 4)$	$(3, 5, 7, 9, 11, 13, 15)$	$(1) \mid (5, 5, 5, 5)$
$(1, 1, 0, 0, 0, 0, 0, 2)$	$(15, 21, 19, 17, 15, 13, 11, 9)$	$(5) \mid (9) \mid (3, 3)$

For the last exceptional parameter

$$a = (1, 0, 0, 0, 0, 0, 0, 0, 0, 0, 1, 1),$$

a positive zero vector is given by spine-edge weights

$$(3, 5, 7, 9, 11, 13, 15, 17, 19, 21, 15)$$

and pendant-edge weights

$$(1) \mid (9) \mid (5).$$

The full list of exact zero-vector certificates, in machine-readable form, is also included in the repository described in Appendix C.

C Reproducibility of the Short-Spine Boundary Computation

This appendix records the exhaustive computer check used for the finite short-spine classification. It is not an additional classification statement; it is a reproducibility record for the tables in Section 5.

The verification code and output files are available in the public repository

<https://github.com/coker412/rt-tree-experiments>

The tables in this manuscript were generated from the repository state identified by the commit

b929c84fd32ac36df789ac7467c42357c0944cfe.

The exact verification is implemented in `code/exact_short_spine_verification.py`. For each $3 \leq m \leq 12$, it enumerates canonical caterpillar parameters, computes the sign of $\lambda_{\max}(R_{T_m(a)})$ using exact rational characteristic polynomials and Sturm root counts, and writes the negative downset, the maximal negative elements, and the first nonnegative boundary to `data/exact_short_spine_verification/`. The tables in Section 5 and Appendix A are read directly from these output files.

The script `code/validate_paper_examples.py` checks the explicit examples and zero-vector certificates appearing in the paper. Its output is recorded in `data/paper_validation/paper_validation.csv`.

The coverage is exhaustive for two reasons. First, every canonical caterpillar parameter with fixed $3 \leq m \leq 12$ is obtained from

$$(1, 0, \dots, 0, 1)$$

by successively adding 1 to coordinates and then re-canonicalizing up to reversal. Second, the negative region is downward closed by Proposition 3.1. Hence the enumeration of all negative children produces the full negative downset and its first nonnegative boundary.

After the full negative downsets have been generated, the zero candidates are obtained by taking all one-step children of the maximal negative elements in Table 1. Every short-spine zero caterpillar lies on this first nonnegative boundary: otherwise it would have a nonnegative immediate predecessor, and Corollary 3.1 would force it to have positive spectral top. The exact Sturm verification then identifies precisely the zero cases listed in Table 2.